Journal of Magnetics 9(2), 27-33 (2004)

Exchange Coupling in Massively Produced $Nd_2Fe_{14}B$+Fe_3B Nanocomposite Powders

Choong Jin Yang[1]*, Eon Byung Park[1], Jong Soo Han[1,2] and Eung Chan Kim[2]

[1]*Research Institute of Industrial Science & Technology (RIST), Nanotechnology Research Lab., Pohang City, P.O. Box 135*
[2]*Dept. of Physics, Youngnam National University, Kyungsan City 214-1*

(Received 7 April 2004)

Magnetic properties of $Nd_4Fe_{77.5}B_{18.5}$ compound in term of exchange coupling between $Nd_2Fe_{14}B$ and Fe_3B magnetic nano crystals in melt spun powders were characterized by varying the quenching speed in mass production line. The exchange coupled phenomenon was characterized as functions of nano crystal size and volume fraction of each magnetic phase which was possible by employing Henkel plot (δM) and refined Mössbauer spectroscopy. The optimized magnetic properties obtained from the present volume production line were: B_r = 11.73 kG, $_iH_c$ = 3.082 kOe, and $(BH)_{max}$ = 12.28 MGOe. The volume fraction of each magnetic phase for those conditions giving the grain size of 10 nm were α-Fe; 4.2%, Fe_3B; 60.1%, and $Nd_2Fe_{14}B$; 35.7%. The superior magnetic properties in the $Nd_2Fe_{14}B$+Fe_3B based nanocomposites were confirmed to be dependant on the volume fraction of Fe_3B.

Key words : nanocomposite permanent magnet, exchange coupling, nanocrystal size, volume fraction

1. Introduction

Following the theoretical and experimental evidences of inter-grain exchange coupling [1, 2], nanocomposite permanent magnetic materials based on both $Nd_2Fe_{14}B$+Fe_3B and $Nd_2Fe_{14}B$+Fe composite phases were attracted much attention due to their enhanced magnetic moment and high energy product as well [3~5]. In economic wise the less use of rare earth element persues the commercial production of nanocomposite magnets capable of reducing the Nd up to 70 wt.%.

Fe_3B+$Nd_2Fe_{14}B$ based nanocomposite materials are obtained from controlling the Nd content of precursor alloy which are produced in amorphous powders followed by optimized heat treatment. During those alloying and annealing process, the hard and soft magnetic phases of $Nd_2Fe_{14}B$ and Fe_3B and/or Fe are nucleated and grown. Accordingly appropriate alloying and following heat treatment are key technologies, because, optimized nano crystal size and their distribution are to be determined during those processes which are essential for the enhanced exchange coupling behavior for both the $Nd_2Fe_{14}B$+Fe_3B and $Nd_2Fe_{14}B$+Fe phased nanocomposites [6~8] via the controlling the quenching speed. It is, therefore, very important to establish appropriate process parameters during nucleation and growth of magnetic phases in the course of annealing the amorphous nanocomposite alloy. Recently a number of studies were carried out to investigate the effect of added element, the presence of interface, and nano crystal size by employing the various experimental tools such as three dimensional atomic probe, DTA, XRD and TEM. Among others computer simulation becomes a convenient tool in predicting the exchange coupling behavior, and actively employed to investigate the character of nanocomposite materials [9~11].

In the present study we report the relationship between the enhanced magnetic properties and appropriate nanocomposite crystals, $Nd_2Fe_{14}B$ and Fe_3B, and their volume fractions. The precursor powders were produced by Plasma Extractive Melt Spinning Process [12] by varying the quenching speed and the following heat treatment. The exchange coupling behavior was characterized by plotting Henkel relationship (δM) [14], and the volume fraction of existing magnetic phases were finely tuned employing Mössbauer spectroscopy.

2. Experimental

Ingots of $Nd_4Fe_{77.5}B_{18.5}$ composition using 99.9% pure Nd and Fe, 99.5% pure B were prepared homogeneously by plasma arc melting under Ar atmosphere. A pilot scale

*Corresponding author: Tel: +82-54-279-6331, e-mail: cjyang@rist.re.kr

of plasma extractive melt spinner was employed to produce in volume production of nanocomposite precursor powders [12]. The quenching speed during spinning of the amorphous powders was varied from 13.2, 19.8 and 26.4 m/sec. The precursor amorphous powders were annealed under vacuum atmosphere of 10^{-5} Torr at the temperature range of 620~710 °C for 10 min.

Magnetic phases formed during quenching and following heat treatment in the melt spun powders were identified by XRD-MXC (Rigaku made) using Cu Kα target using Ni filter. DTA (differential thermal analysis) was used to investigate the magnetic transformation as a function of temperature. All the magnetic properties were characterized using vibrating sample magnetometer (Toei made) applying the external field of 16 kOe in the plane direction of those sample powders. Especially, AGM (alternating gradient magnetometer: Princeton made) was utilized in plotting DC demagnetization curves and isothermal AC remanence curves of interested samples to obtain δM figures which demonstrate the exchange coupling behavior well. Mössbauer spectroscopy (Fast Comtec made) was used in confirming the volume fraction of each magnetic phase using the γ-ray source of Rh dopped by 30 mCurie ^{57}Co.

3. Results and Discussion

3.1. Nucleation and growth of magnetic phases during quenching and heat treatment

This study was started in recognition of the importance that the cooling speed determines the grain size and its volume fraction of precursor amorphous powders. Accordingly the nucleation and growth behaviors of each $Nd_2Fe_{14}B$ and Fe_3B (and Fe) phase were carefully controlled by varying the quenching speed during melt spinning (13.2, 19.8, 26.4 m/sec), and heat treatment temperature at the appropriate range (620~710 °C). The first nucleation activity determines the intial grain size of the firstly formed phase, and the duration of heating will influence the growth of the phase present and newly formed phase.

Fig. 1 summarizes the magnetic properties measured from melt spun powders followed by post annealing as in the figures. Most interesting point is that the best magnetic properties in terms of $_iH_c$, B_r and $(BH)_{max}$ are obtained from the powders spun at the quenching speed of 19.8 m/sec all the time, and heat treated at 650 °C, generally. Resultantly the quenching (19.8 m/sec) and annealing (650 °C/10 min) conditions during the volume production process are confirmed to be most appropriate in activating the exchange coupling between $Nd_2Fe_{14}B$ and Fe_3B grains. Fig. 1 shows that the post annealing above 650 °C deteriorates the magnetic properties. The previous study performed by the same authors [4, 5] reported that nanocomposite of $Nd_2Fe_{14}B$+Fe_3B based on NdFeCoGaZrB composition with the nano crystal size of 18~20 nm after annealing the compounds at 680 °C for 10 min exhibited the maximum properties. At the present volume production process the detailed field emission TEM photograph shows in Fig. 2(a) that much finer grain size below 10 nm of $Nd_2Fe_{14}B$ phase in uniform distribution after appropriate process, 650 °C/10 min, was measured. However, the grains seem to grow very rapidly by increasing the annealing temperature up to 710 °C, which resulted in 50 nm size as shown in Fig. 2(b). The best magnetic properties obtained from the powders with the composition of $Nd_4Fe_{77.5}B_{18.5}$ spun at 19.8 m/sec followed by annealing at 650 °C for 10 min were: $_iH_c$ = 3.082 kOe, B_r = 11.73 kG, and $(BH)_{max}$ = 12.28 MGOe. Therefore the grain size of 10 nm seems to be the target value to be observed in the volume production process for $Nd_4Fe_{77.5}B_{18.5}$ composition.

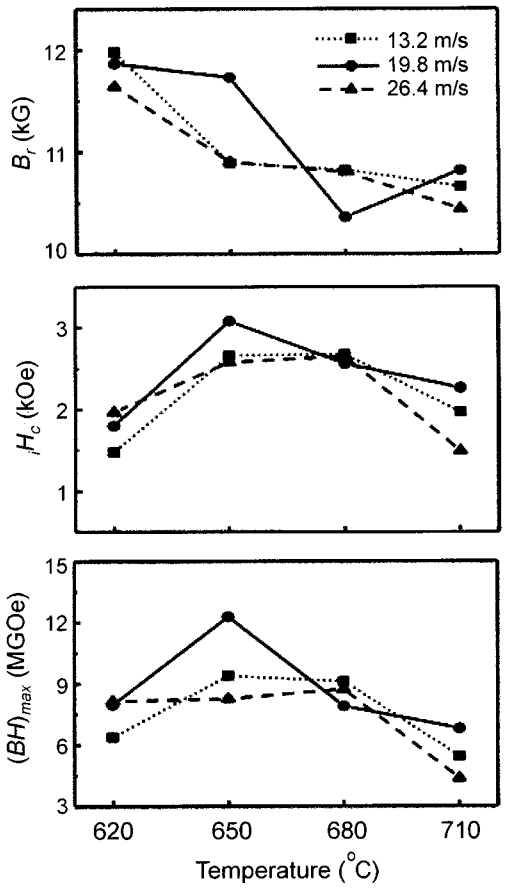

Fig. 1. The effect of cooling rate on Magnetic properties of $Nd_4Fe_{77.5}B_{18.5}$ ribbons as a function of annealing temperature.

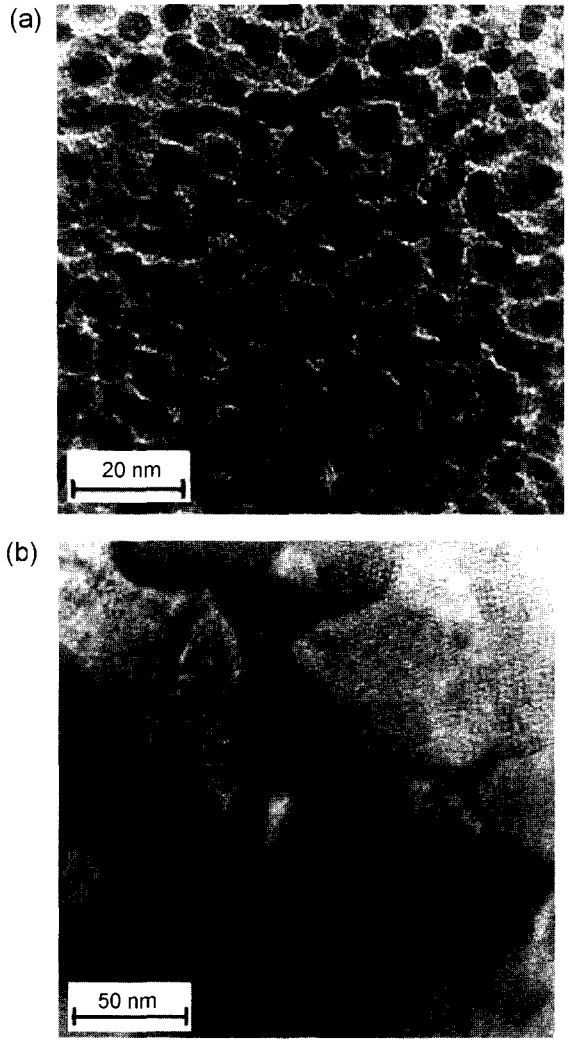

Fig. 2. Field emission TEM photographs showing the nano crystal in the powders spun at 19.8 m/sec and then heat treated at (a) 650 °C, and (b) 710 °C for 10 min.

The effect of quenching speed and post annealing treatment was characterized in detail by examining the nucleation and growth behavior of those magnetic phases during transformation using DTA, and the phases were identified using x-ray diffraction pattern. Fig. 3 indicates that basically $Nd_2Fe_{14}B$ and Fe_3B phases formed as the main elements regardless of quenching rate, however, the formation of α-Fe seems not to be prominent. In the course of heating the amorphous melt spun powders, Fe_3B firstly form around 590 °C as can be seen in Fig. 4, and the formation of $Nd_2Fe_{14}B$ takes place around 650 °C. However, as the melt spinning speed is increased the nucleation of Fe_3B tends to take place at higher temperature side, by 5 °C in general, while the nucleation of $Nd_2Fe_{14}B$ moves to lower temperature side, 2~3 °C

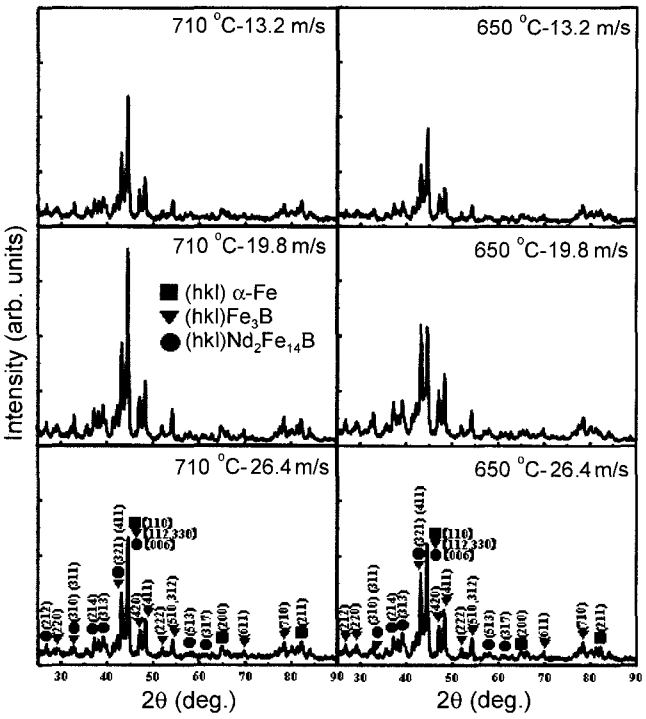

Fig. 3. X-ray diffraction patterns of $Nd_4Fe_{77.5}B_{18.5}$ ribbons spun at denoted cooling rate.

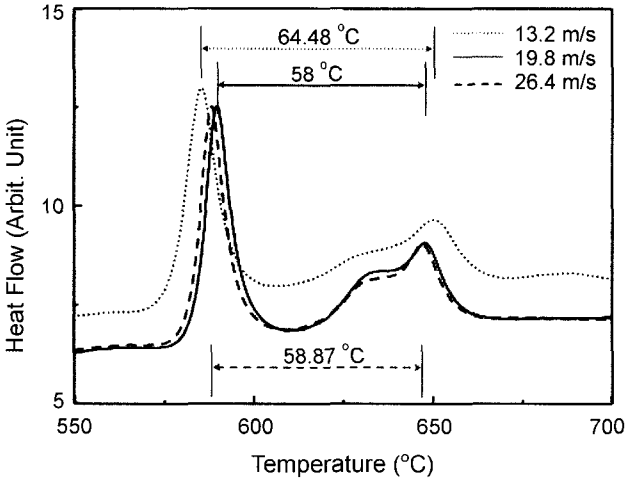

Fig. 4. Crystallization behaviors of $Nd_4Fe_{77.5}B_{18.5}$ ribbons spun at the denoted cooling rate.

lower in general. Accordingly, the interval between those transformations of two magnetic phases becomes smaller, and the short interval causes an uniform distribution of grain sizes of each phase. Fig. 4 suggests that the powders spun at 19.8 m/sec, which shows the nucleation interval between $Nd_2Fe_{14}B$ and Fe_3B is only 58 °C, would exhibit a most uniform grain size distribution.

3.2. Exchange coupling of $Nd_2Fe_{14}B+Fe_3B$ nanocomposite characterized by Mössbauer spectroscopy and Henkel plot

If one can measure isothermal ac remanence curves ($I_r(H)$) and dc demagnetization curves ($I_d(H)$) of the nanocomposite materials, the degree of exchange coupling can be examined by plotting $M(H)$ curves defined in terms of Wohlfarth's single domain particle model as follow [13]:

$$I_d(H) = I_r(\infty) - 2I_r(H) \quad (1)$$

The relationship was proposed for the particles in the range of single domain without any interaction between them. Later on Kelly *et al.* [14] extended the relationship into exchange coupled particles such as nanocomposite magnetic materials using the term of coercivity difference measured from $I_r(H)$ and $I_d(H)$ curves:

$$I_d(H)/I_r(H) = 1 - 2I_r(H)/I_r(8) + \delta M(H) \quad (2)$$

Accordingly $\delta M(H)$ denotes the magnitude of the coercivity difference in the course of magnetization reversal. It is known that positive $\delta M(H)$ happens when exchange coupling is predominant, on the contrary, $\delta M(H)$ is negative when magnetostatic is major reaction between those particles. Fig. 5 shows those exchange coupled behaviors of $Nd_2Fe_{14}B+Fe_3B$ nanocomposite particles made at various quenching speed. In general, the exchange coupling of measured materials made at different quenching speed exhibits identical behaviors. However, samples annealed at 650 °C shows the most prominent peaks in both the positive and negative directions which is confirming that annealing at 650 °C for 10 min endows the most appropriate condition. In Fig. 5 showing those $\delta M(H)$ curves, a transition from positive to negative along the curve takes place. This transition point corresponding to coercivity value of each material also shows the higher value for the material annealed at 650 °C for 10 min than those at 710 °C for 10 min. Those mentioned observations are all identical to those values summarized in Fig. 1, especially for the materials quenched at 19.8 m/sec. The refined analysis in term of $\delta M(H)$ plotting is exactly identical to the measured coercivity and remanence values for the appropriate conditions.

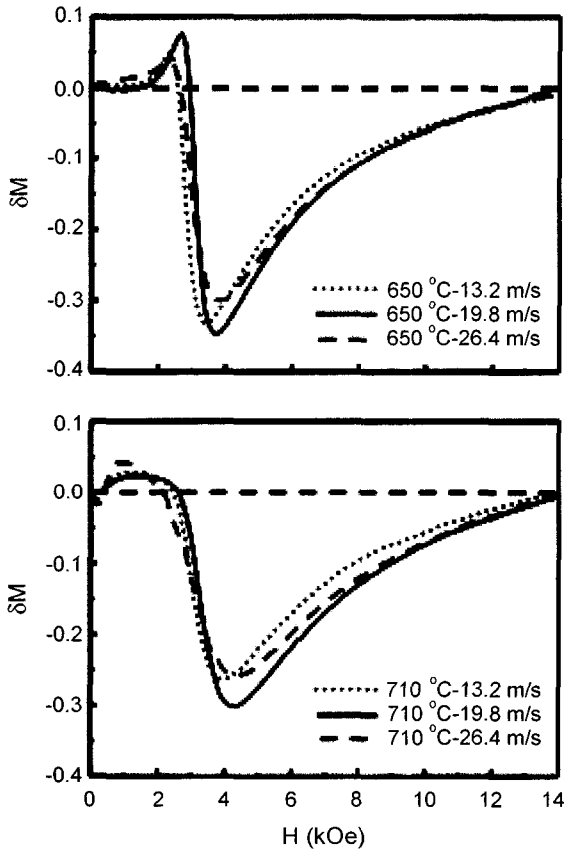

Fig. 5. Henkel plot of $Nd_4Fe_{77.5}B_{18.5}$ ribbons at the denoted cooling rate.

In order to investigate the volume fraction of each $Nd_2Fe_{14}B$ and Fe_3B phase, Mössbauer spectrum for the nanocomposite precursor quenched at 13.2, 19.8, and 26.4 m/sec and then annealed at 650 °C for 10 min was obtained, and the finely analyzed spectrum is demonstrated in Fig. 6(a), (b), and (c). Fe_3B unit cell of body centered tetragonal crystal has three nonequivalent site of Fe atoms. Fe I(8g) and Fe II(8g) sites are of ten Fe atoms neighbored with three B atoms, and Fe III(8g) site is of ten Fe atoms neighbored with four B atoms at the vertices of the trigonal prism [15]. Around those three nonequivalent Fe site exchange coupling between B-B, Fe-B, and Fe-Fe atoms is not equivalent due to their different interatomic distances. $Nd_2Fe_{14}B$ unit cell of tetragonal structure is well known which has six different nonequivalent Fe atomic sites defined as k_1, k_2, j_1, j_2, e, and c [18].

The hyperfine filed of Fe atoms in the case of 3d transition metal or compounds such as Fe_3B and $Nd_2Fe_{14}B$ is assumed to arise from three conditions [15]: (1) a core polarization due to exchange interaction between the on-site moment of the 3d electrons and their s electrons, (2) a spin polarization of the conduction s electrons due to the on-site moment of the atom itself, and (3) an overall conduction electrons polarization due to the moments in neighboring shells. Generally the first two (1) and (2) items are proportional to the on-site magnetic moment, while the (3) item is proportional to the number of its nearest neighbors [15]. For the hyperfine field at the Fe nuclei in the present spectroscopic study, the magnitude of magnetic moment from the nearest neighboring site is

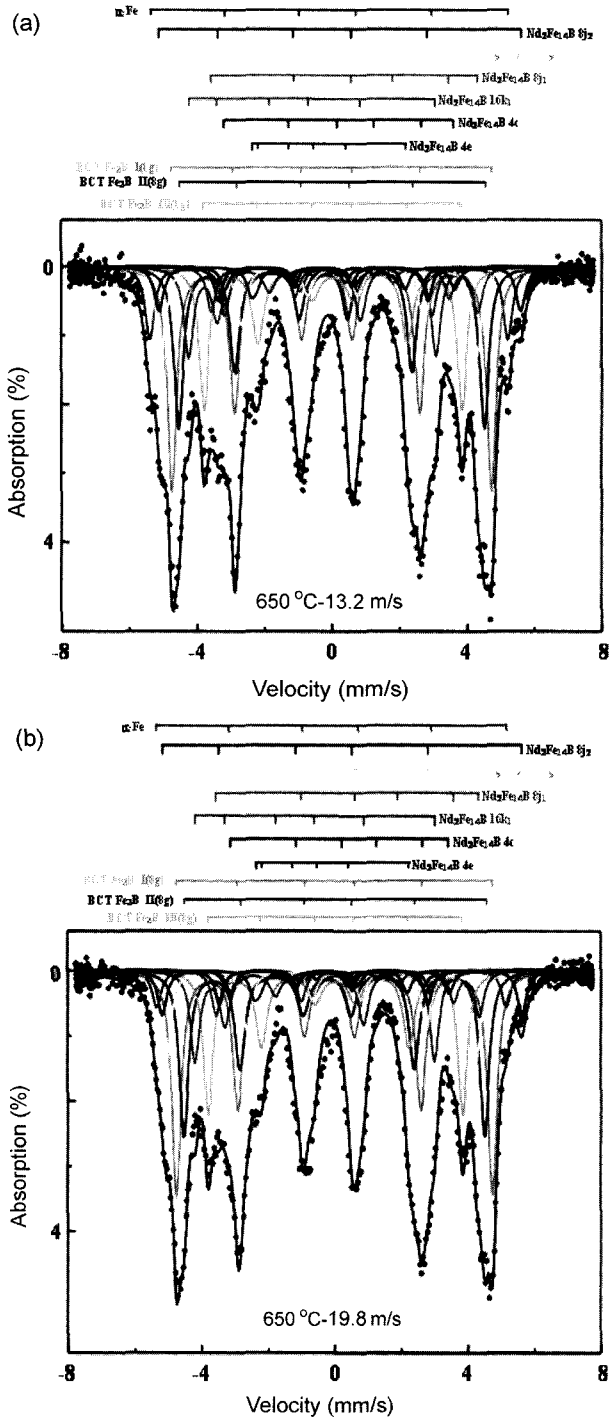

Fig. 6. Refined Mössbauer spectra of melt-spun $Nd_4Fe_{77.5}B_{18.5}$ ribbons. (a) at the quenching speed of 13.2 m/sec and then heat treated at 650 °C for 10 min. (b) spun powders at the quenching speed of 19.8 m/sec.

assumed to be very small compared with the contributions from on-site moment.

Accordingly, the authors quoted the measured value of hyperfine field for bct Fe_3B unit cell coming from the on-

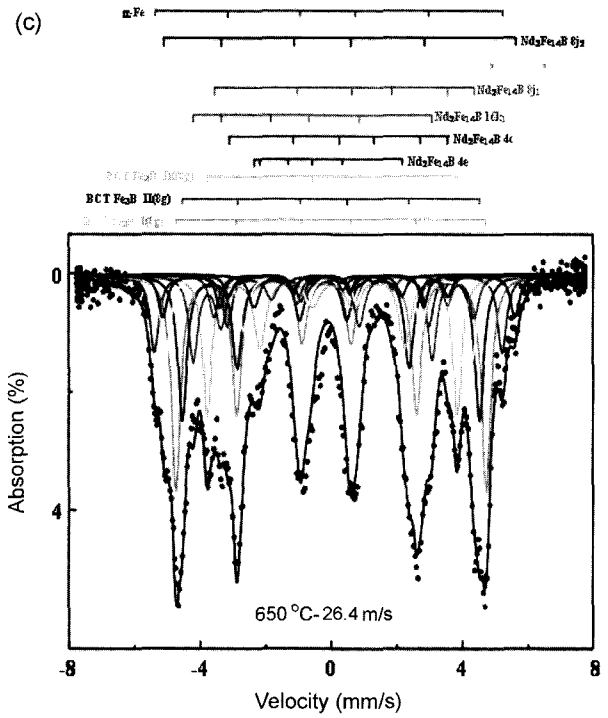

Fig. 6. (c) spun powders at quenching speed of 26.4 m/sec.

site magnetic moment, and used the reported value of 150 kOe/μ_B [15] for the present study. Also by using the atomic magnetic moment of 2.03, 1.89, and 1.61 μ_B for Fe I(8g), Fe II(8g), and Fe III(8g), respectively, the authors estimated the magnitude of hyperfine filed for those three nonequivalent sites in the order of Fe I(8g) > Fe II(8g) > Fe III(8g). Besides, Taylor and Gangulee [16] proposed that the magnetic moment of Fe atom in Gd(or Nd)-Fe-B compounds can be described as:

$$\mu_{Fe}(\mu_B) = 2.6–2.1(\chi_{Nd}/\chi_{Fe})–2.4(\chi_B/\chi_{Fe}) \quad (3)$$

where χ_{Fe}, χ_{Nd} and χ_B are number of Fe, Nd and B atoms, respectively. Therefore, the authors also could quote the above relationship to calculate the magnitude of hyperfine field of each site for $Nd_2Fe_{14}B$ unit cell, and estimated in the order of $4e < 4c < 16k_1 < 8j_1 < 16k_2 < 8j_2$ [17~20].

Mössbauer spectrum was analyzed elaborately using Fast Comtec's PC-MOS II program. Sub-spectrums of those all the nonequivalent Fe atomic sites in Fe_3B, $Nd_2Fe_{14}B$, and α-Fe were assumed to have identical line widths. Likewise the temperature dependency of probability that Fe atoms would not show recoiling was also assumed to be the same for all the Fe atomic sites. Since powder samples were used for the present analysis the relative intensities from each sub-spectra were assumed to have the intensity ratio $I_1 : I_2 : I_3 : I_4 : I_5 : I_6 = 3 : 2 : 1 : 1 : 2 : 3$ of the Zeeman line [17]. Since the unit cell of tetragonal

Table 1. Summary of Mössbauer spectroscopy

Phase/site		HF (T)			IS (mm/s)			QD (mm/s)			Vol (%)		
Quenching rate		13.2 m/s	19.8 m/s	26.4 m/s	13.2 m/s	19.8 m/s	26.4 m/s	13.2 m/s	19.8 m/s	26.4 m/s	13.2 m/s	19.8 m/s	26.4 m/s
BCC α-Fe		32.88	32.57	32.88	-0.085	-0.104	-0.079	0.021	0.03	0.008	8	4.2	8.9
BCT Fe_3B	$Fe_{(I)}$(8g)	29.34	29.43	29.33	-0.063	-0.07	-0.061	0.139	0.154	0.138	24.5	25.3	24.6
	$Fe_{(II)}$(8g)	28.05	28	28.07	-0.119	-0.108	-0.119	0.235	0.216	0.232	17.6	18.7	16.5
	$Fe_{(III)}$(8g)	23.69	23.7	23.63	0.041	0.03	0.043	0.007	0.01	-0.006	15.6	16.1	15.8
Tetragonal $Nd_2Fe_{14}B$	Fe(16k_1)	22.7	22.3	22.58	-0.91	-0.893	-0.895	0.698	0.317	0.695	9.8	10.2	9.8
	Fe(16k_2)	28.98	28.86	28.97	-0.162	-0.159	-0.159	-0.399	-0.455	-0.4	9.8	10.2	9.8
	Fe(8j_1)	24.47	24.51	24.6	0.795	0.849	0.828	-0.811	-0.895	-0.859	4.9	5.1	4.9
	Fe(8j_2)	33.21	33.51	33.28	0.0002	-0.046	-0.02	0.496	0.554	0.525	4.9	5.1	4.9
	Fe(4c)	21.09	20.32	20.68	0.487	0.464	0.504	-0.471	-0.595	-0.561	2.45	2.55	2.4
	Fe(4e)	14.12	14.25	14.12	-0.505	-0.512	-0.535	0.809	0.793	0.837	2.45	2.55	2.4

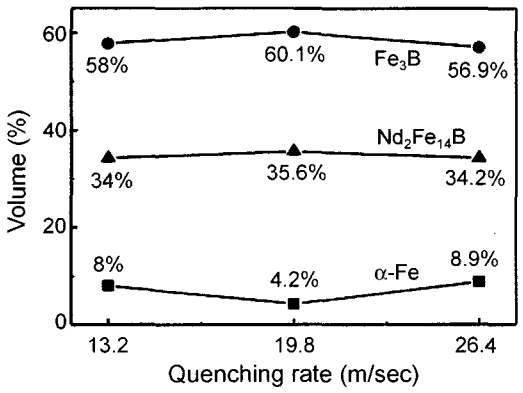

Fig. 7. Variation of volume fraction of melt-spun $Nd_4Fe_{77.5}B_{18.5}$ ribbons spun at the various cooling rate.

$Nd_2Fe_{14}B$ has six different nonequivalent Fe atomic sites known as k_1, k_2, j_1, j_2, e, and c, and is known to have 16, 16, 8, 8, 4, and 4 Fe atoms at each site, the authors fitted sub-spectrum curves using the area ratio of 4 : 4 : 2 : 2 : 1 : 1 for each site, respectively. Table 1 summarizes the result of Mössbauer spectroscopy.

The total volume fraction of each $Nd_2Fe_{14}B$, Fe_3B and α-Fe is denoted in Fig. 7 as a function of quenching speed. The highest volume fraction of $Nd_2Fe_{14}B$ and Fe_3B are 35.7 and 60.1%, respectively, and obtained from the materials quenched at 19.8 m/sec and then annealed at 650 °C for 10 min. More interesting behavior of those variations in volume fraction is that the variation of magnetically hard $Nd_2Fe_{14}B$ is not prominent, however, the variation of Fe_3B shows a peak value at 19.8 m/sec and then decreased at the speed lower or higher than 19.8 m/sec. The variation behavior for α-Fe is exactly opposite to that of Fe_3B. Accordingly the appropriate process parameters giving the best magnetic properties for the present volume production are based on the abundant formation of Fe_3B at the expense of α-Fe.

4. Conclusion

Permanent magnetic properties of nanocomposite $Nd_4Fe_{77.5}B_{18.5}$ compound is confirmed to be sensitively influenced by the size of each magnetic phase $Nd_2Fe_{14}B$ and Fe_3B present and their size distribution. Basically the exchange coupling behavior plays a key role for the enhancement of magnetic moment of the nanocompposite material based on $Nd_2Fe_{14}B$+Fe_3B composition, and the overall properties were observed to be dependant on the volume fraction of each phase. Those magnetic properties were characterized as functions of nano crystal size and volume fraction of each magnetic phase which was possible by employing Henkel plot (δM) and refined Mössbauer spectroscopy. The optimized magnetic properties obtained from the present volume production line were: B_r = 11.73 kG, ${}_iH_c$ = 3.082 kOe, and $(BH)_{max}$ = 12.28 MGOe. The volume fraction of each magnetic phase for those conditions giving the grain size less than 10 nm were α-Fe; 4.2%, Fe_3B; 60.1%, and $Nd_2Fe_{14}B$; 35.7%, respectively.

References

[1] R. Skomski and J. M. D. Coey, IEEE. Trans. Magn. **29**, 2860 (1993).
[2] R. Fisher, T. Schrefl, H. Kronmüler, and J. Fidler, J. Magn. Magn. Mater. **153**, 35 (1996).
[3] G. C. Hadjipanayis and W. Gong, J. Appl. Phys. **64**, 5559 (1988).
[4] C. J. Yang and E. B. Park, J. Magn. Magn. Mater. **186**, (1997) 243.
[5] C. J. Yang, E. B. Park, Y. S. Hwang, and E. C. Kim, IEEE. Trans. Magn. **35**, 3328 (1999) 8.
[6] Z. H. Cheng, B. G. Shen, M. X. Mao, J. J. Sun, F. W. Wang, and Y. D. Zhang, J. Phys. **7**, 3949 (1995).
[7] L. X. Liao, Z. Altounian, and D. H. Ryan, Phys. Rev. B. **47**, 230 (1993).

[8] J. M. Breton and S. Steyaert, J. Phys. **11**, 4941 (1999).
[9] J. Panagiotopoulos, L. Withanawasam, and G. C. Hadjipanayis, J. Magn. Magn. Mater. **152**, 353 (1996).
[10] T. Schrefl and J. Fidler, IEEE. Trans. Magn. **35**, 3223 (1999).
[11] T. Schrefl, H. F. Schmidts, J. Fidler, and H. Kronmüler, J. Magn. Magn. Mater. **124**, 251 (1993).
[12] C. J. Yang, E. B. Park, and S. D. Choi, Mat. Let. **24**, 347 (1995).
[13] E. P. Wohlfarth, J. Appl. Phys. **29**, 595 (1958).
[14] P. E. Kelly, K. O. Grady, P. I. Mayo, and R. W. Chantrell, IEEE. Trans. Magn. **25**(5), 3881 (1989).
[15] Y. D. Zhang, J. I. Budnick, J. C. Ford, and W. A. Hines, J. Magn. Magn. Mater. **100**, 13 (1991).
[16] R. C. Taylor and A. Gangulee, J. Appl. Phys. **53**, 2341 (1982).
[17] R. Kamal and Y. Andersson, Phys. Rev. B. **32**, 1756 (1985).
[18] J. F. Herbst and J. J. Croat, Phys. Rev. **29**, 29 (1994).
[19] C. B. Shoemaker, D. P. Shoemaker, and R. Fruchart, Acta Cryst. **C40**, 1665 (1984).
[20] D. Givord, H. S. Li, J, and M. Moreau, Sol. Stat. Comm. **50**, 497 (1984).